F. Nelli, L.G. Bennetts, D.M. Skene, J.P. Monty, J.H. Lee, M.H. Meylan, A. Toffoli
Reflection and transmission of regular water waves by a thin, floating plate
Wave Motion, 2017; 70:209-221

Reflection and transmission of regular water waves by a thin, floating plate

Nelli F.[a], Bennetts L.G.[b], Skene D.M.[b], Monty J.P.[c], Lee J.H.[c], Meylan M.H.[d], Toffoli A.[e]

[a]*Centre for Ocean Engineering Science and Technology, Swinburne University of Technology, Hawthorn, VIC, Australia*
[b]*School of Mathematical Sciences, University of Adelaide, Adelaide, SA, Australia*
[c]*Department of Mechanical Engineering, University of Melbourne, Melbourne, VIC, Australia*
[d]*School of Mathematical and Physical Sciences, University of Newcastle, Callaghan, NSW, Australia*
[e]*Department of Infrastructure Engineering, University of Melbourne, Melbourne, VIC, Australia*

Abstract

Measurements of the wave fields reflected and transmitted by a thin floating plastic plate are reported for regular incident waves over a range of incident periods (producing wavelengths comparable to the plate length) and steepnesses (ranging from mild to storm-like). Two different plastics are tested, with different densities and mechanical properties, and three different configurations are tested. The configurations include freely floating plates, loosely moored plates (to restrict drift), and plates with edge barriers (to restrict waves overwashing the plates). The wave fields reflected and transmitted by plates without barriers are shown to become irregular, as the incident waves become steeper, particularly for the denser plastic and the moored plate. Further, the proportion of energy transmitted by the plates without barriers is shown to decrease as the incident wave becomes steeper, and this is related to wave energy dissipation.

Keywords: Ocean waves; Thin plate; Energy dissipation.

1. Introduction

Thin, floating plates have been used to model sea ice floes (discrete chunks of sea ice) and very large floating structures (VLFSs, e.g. floating runways), with a large branch of these models developed to investigate interactions between surface-water waves and the plates (floes or VLFSs). For these applications, typically, the horizontal dimensions of the plates are comparable to wavelengths, so that the plates flex in response to the waves, in addition to experiencing rigid-body motions. Particularly for sea ice applications, wave–plate interaction models are used to predict the proportions of incident wave energy reflected and transmitted by the floe, as this provides predictions of the distances ocean waves travel

*Corresponding author: F. Nelli, Centre for Ocean Engineering Science and Technology, Swinburne University of Technology, P.O.Box 218, Hawthorn, VIC 3122, Australia. (fnelli@swin.edu.au)

into the ice-covered ocean and impact the ice cover (Bennetts and Squire, 2012, Williams et al., 2013a,b).

The canonical theoretical wave–plate interaction model is a Kirchoff–Love thin-plate floating on top of an inviscid, incompressible fluid undergoing irrotational motions, meaning the water velocity field can be defined as the gradient of a scalar potential function. It assumes linearity (in terms of the Bernoulli water pressure, the material response of the plate, and the moving boundary conditions) and harmonic time dependence at a prescribed angular frequency $\omega = 2\pi/\tau$, thus fixing the open-water wavelength λ (for a given water depth). The plate oscillates in response to an incident wave at the prescribed frequency, in both its rigid-body and flexural modes, but does not drift. Water and plate motions are coupled at the lower surface of the plate only, assuming that all points on this surface remain in contact with the water during motion. This produces a boundary-value problem for the time-independent component of the velocity potential, ϕ, in which the plate cover provides a high-order surface condition, effectively removing the vertical geometry of the plate from the problem. Reflection and transmission result solely from impedance mismatches (i.e. different wave numbers) between the open water and the plate-covered water.

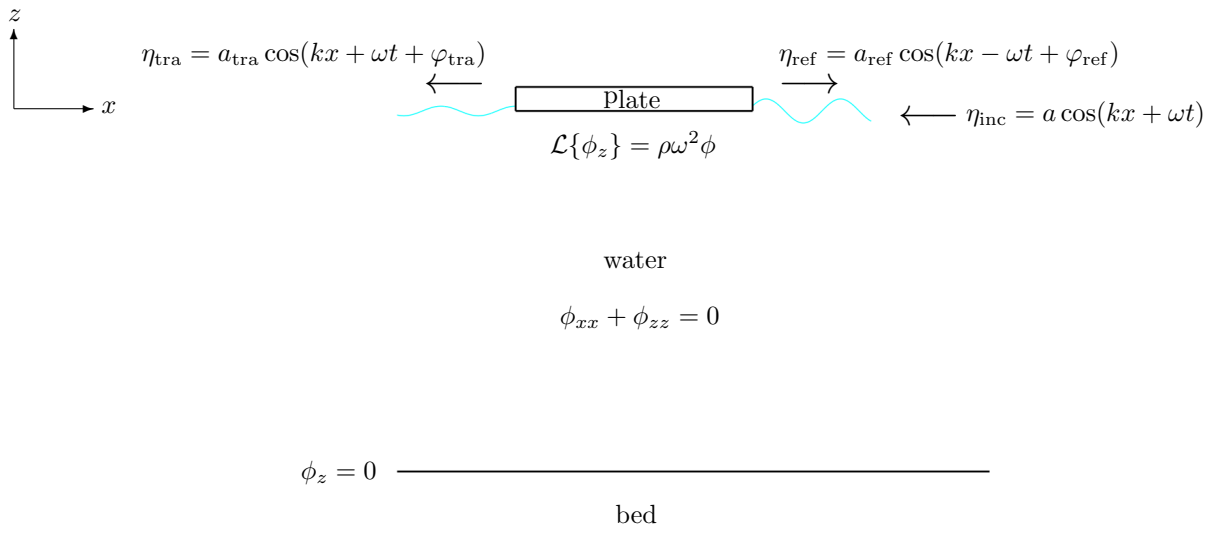

Figure 1: Schematic of the two-dimensional canonical model and governing equations of the associated boundary-value problem.

Meylan and Squire (1994) studied wave reflection and transmission by an ice floe of uniform thickness h, using a two-dimensional version of the canonical model (one horizontal dimension and one depth dimension, with coordinates x and z, respectively), similar to the theoretical model used in this study, although neglecting draught of the plate and its surge motion. Fig. 1 shows a schematic of the two-dimensional canonical model and the associated boundary-value problem for ϕ. The operator $\mathcal{L}$ involved in the surface condition is defined as $\mathcal{L}\{\bullet\} = \rho g$ for the intervals of open water, where ρ is the water density and $g \approx 9.81\,\mathrm{m\,s^{-2}}$ is the constant of gravitational acceleration. For the interval occupied by the plate, it is

defined by

$$\mathcal{L}\{\bullet\} = (\rho g - \omega^2 m)\,\bullet + \frac{Eh^3 \bullet_{xxxx}}{12(1-\nu^2)} \tag{1}$$

where m is the plate mass per unit length, E is its Young's modulus and ν is its Poisson's ratio. Free edge conditions, $\phi_{xxz} = 0$ and $\phi_{xxxz} = 0$, are applied at the ends of the plate.

Motion is forced by a train of regular waves (with sinusoidal profiles), incident on the plate from its right-hand side, with surface elevation $\eta_{\text{inc}} = a\cos(kx + \omega t)$, where a is a prescribed amplitude and $k = 2\pi/\lambda$ is the open-water wave number. The plate partially reflects and partially transmits the incident waves. Far enough away from the plate that the exponentially decaying local motions have died out, the reflected and transmitted fields are regular wave trains, with surface elevations

$$\eta_{\text{ref}} = a_{\text{ref}}\cos(kx - \omega t + \varphi_{\text{ref}}) \qquad \text{and} \qquad \eta_{\text{tra}} = a_{\text{tra}}\cos(kx + \omega t + \varphi_{\text{tra}}), \tag{2}$$

respectively, where a_{ref} and a_{tra} are the reflected and transmitted amplitudes, and φ_{ref} and φ_{tra} are phases. In the front field, on the right-hand side of the plate, the incident and reflected waves superpose to create a partial standing wave field. In the rear field, on the left-hand side, the wave field consists of transmitted waves only.

The canonical model is energy conserving, meaning that the energy in the incident waves is distributed into the reflected and transmitted waves. This property is expressed as $R + T = 1$, where $R = |a_{\text{ref}}/a|^2$ and $T = |a_{\text{tra}}/a|^2$ — the proportions of energy reflected and transmitted — are referred to as the reflection and transmission coefficients, respectively.

Meylan and Squire (1994) found that R is generally less than order 10^{-2} for plate lengths less than approximately one-third the incident wavelength, implying that the incident wave is almost entirely transmitted in this regime. Longer plates were found to reflect much greater proportions of the incident waves, with values of R typically order 10^{-1}, although periodically vanishing as the plate length increased, due to resonance.

Montiel et al. (2012) showed that, for a plate with properties similar to those considered in this study although only half as thick, including the Archimedean draught of the plate in the model affects reflection for incident wavelengths approximately less than half the plate length only. Bennetts et al. (2007) and Smith and Meylan (2011) showed examples of the impacts of thickness variations on reflection and transmission.

Meylan and Squire (1996) used the canonical model with a circular disk to study wave scattering (reflection/transmission over all horizontal directions) by an ice floe, noting that Masson and LeBlond (1989) earlier calculated scattering by a rigid circular floe. They found that, as the plate diameter increases with respect to the incident wavelength, the scattered energy increasingly focusses around the reflected and transmitted directions. Similarly, for elliptical plates, Bennetts and Williams (2010) found that directional scattering tends to pure reflection/transmission as the width of the plate increases.

Bennetts et al. (2015) used a laboratory experimental model, akin to the canonical theoretical model, to study transmission of regular incident waves by an ice floe. The experiments involved measurements of the surface elevation in the rear field of a loosely moored, square, plastic plate, with regular incident waves, for a range of plate thicknesses,

incident wave periods and steepnesses, and two plastics. They showed that for incident steepnesses as small as $ka = 0.08$, the plate could transmit highly irregular waves (in this case inducing a broad frequency content), with the irregularity increasing as the incident waves became steeper. They attributed this phenomenon to incident waves washing over the upper surface of the plate due to its small freeboard (referred to as overwash), then running off the plate into the rear field, producing high-frequency components in the transmitted wave spectrum. Overwash is a highly nonlinear phenomenon not included in the canonical model, but commonly noted in laboratory tests on wave interactions with thin floating plates/experimental models of wave-ice interactions (e.g. Montiel et al., 2013b,a, McGovern and Bai, 2014, Yiew et al., 2016, Sree et al., 2016), and with Massom and Stammerjohn (2010) reporting observations of seawater being washed onto the surfaces of Antarctic sea ice floes. Skene et al. (2015) analysed the depth of the overwash during Bennetts et al. (2015)'s experiments, using measurements provided by a wave gauge mounted on top of the plate, and developed an associated theoretical model, using predictions of plate motions and wave surface elevations surrounding the plate provided by the canonical model.

Bennetts and Williams (2015) studied transmission of regular incident waves through arrays of 40–80 loosely moored, circular, wooden plates during a series of laboratory wave-basin experiments. They showed that, for short incident periods, the proportion of wave energy transmitted drops sharply as the wave steepness increases, noting a correlation between this behaviour and the occurrence of overwash. Similarly, Meylan et al. (2014) used measurements of wave activity in the ice-covered Antarctic Ocean to provide evidence that the energy of short-period waves attenuate more rapidly with distance travelled as the incident steepness increases.

Toffoli et al. (2015) analysed transmission of regular incident waves by an unmoored plastic plate in a laboratory–experimental setting, replicating the two-dimensional version of the canonical model. They showed the theoretical model (including draught and surge) predicts transmitted amplitudes accurately for incident waves with steepness approximately $ka \leq 0.06$ only, and increasingly over predicts the transmitted amplitudes as the incident waves become steeper. Further, by extracting the reflected wave energy from surface-elevation measurements in the front field, they showed that the loss of model accuracy is correlated to wave-energy dissipation in the experiments, indicating wave breaking in the overwash as the likely sink.

An extended experimental dataset to that of Toffoli et al. (2015) is analysed in this investigation. The dataset includes tests on loosely moored plates (similarly to Bennetts et al., 2015, Bennetts and Williams, 2015), and plates with barriers around their edges to prevent overwash, respectively, to test the roles of drift and overwash on reflection and transmission. Moreover, it includes data from two different plastics, with different mechanical properties, and different densities (providing different freeboards and affecting the strength of overwash). The reflected wave field is explicitly analysed, in addition to the transmitted wave field. It is shown that the reflected and transmitted fields are regular for the plates with barriers, but become irregular as the incident steepness increases for the plates without barriers, with the irregularity stronger for the denser plate and when the plate is moored. The reflection coefficients produced by the unmoored plates are shown to be significantly

smaller than those produced by the moored plates, for all but the longest-period incident waves tested. Consistent with the findings of Toffoli et al. (2015), the transmission coefficients are found to decrease with increasing incident steepness, but only for the plates without barriers. Evidence is provided to link the decrease in transmission coefficients with wave-energy dissipation.

2. Experimental setup and post processing

Experimental tests were conducted in the 60 m long and 2 m wide Extreme Air-Sea Interaction Flume, University of Melbourne, Australia. The flume is equipped with a cylinder-type wave-maker at one end, and a linear beach at the opposite end. The flume was filled with fresh water (density $\rho \approx 1000\,\mathrm{kg\,m^{-3}}$) up to a depth of 0.9 m.

A 1 m long, 1.9 m wide and 0.01 m thick plastic sheet was placed in the flume, to act as the thin plate. Two different plastics were tested: (i) polypropylene (PP)[1] with density $\rho_{\mathrm{pl}} = 905\,\mathrm{kg\,m^{-3}}$ (similar to the density of sea ice) and Young's modulus $E = 1.6\,\mathrm{GPa}$, and (ii) polyvinyl chloride (PVC) foam[2] with $\rho_{\mathrm{pl}} = 569\,\mathrm{kg\,m^{-3}}$ and $E = 500\,\mathrm{MPa}$, making it lighter and more flexible than the PP. A Poisson's ratio of $\nu = 0.4$ is used for both PP[3] and PVC (see Newman and Strella, 1965).

The dynamic pressure of the most energetic incident wave used during the tests (period $\tau = 1\,\mathrm{s}$ and amplitude $ka = 0.15$) is $\sim 400\,\mathrm{Pa}$. According to Deshpande and Fleck (2001), PVC has an elastic response to stresses lower than 4 MPa, justifying comparisons to a linear elastic model. Similarly, according to Shokrieh et al. (2015), PP has an elastic response to stresses lower than 15 MPa. Moreover, in a related study, Meylan et al. (2015) showed the canonical model accurately predicts the motions of PVC and PP plates under forcing from regular waves with periods and steepnesses similar to those used in this study (defined below).

Fig. 2 shows plan-view schematics of three different configurations used for the tests. The top panel shows the case in which the plate is freely floating, so that it drifts downstream during the tests. The middle panel shows the case in which the plate is loosely moored, to allow surge but restrict drift. (The left-hand panel of Fig. 3 shows a photo of the moored PVC plate.) The bottom panel shows the case in which the plate is moored and has lightweight barriers around its edges, to prevent overwash. (The right-hand panel of Fig. 3 shows a photo of the moored PVC plate with barriers.)

The wave-maker was used to generate regular (monochromatic) incident wave trains. For each plastic and deployment, three different wave periods, $\tau = 2\pi/\omega$, were used: $\tau = 0.8\,\mathrm{s}$ (corresponding to a wavelength $\lambda = 1\,\mathrm{m}$); $\tau = 0.9\,\mathrm{s}$ ($\lambda = 1.26\,\mathrm{m}$); and $\tau = 1\,\mathrm{s}$ ($\lambda = 1.56\,\mathrm{m}$). For each period, five different amplitudes were imposed to give wave-steepness values $ka =$

[1] a general datasheet can be found at `http://www.efunda.com/materials/polymers/properties/polymer_datasheet.cfm?MajorID=pp&MinorID=1`

[2] `http://astrup.no/content/download/4647/16242/version/1/file/PVC+Forex+Classic+Datablad.pdf`

[3] `http://engr.bd.psu.edu/rxm61/METBD470/Lectures/PolymerProperties20from20CES.pdf`

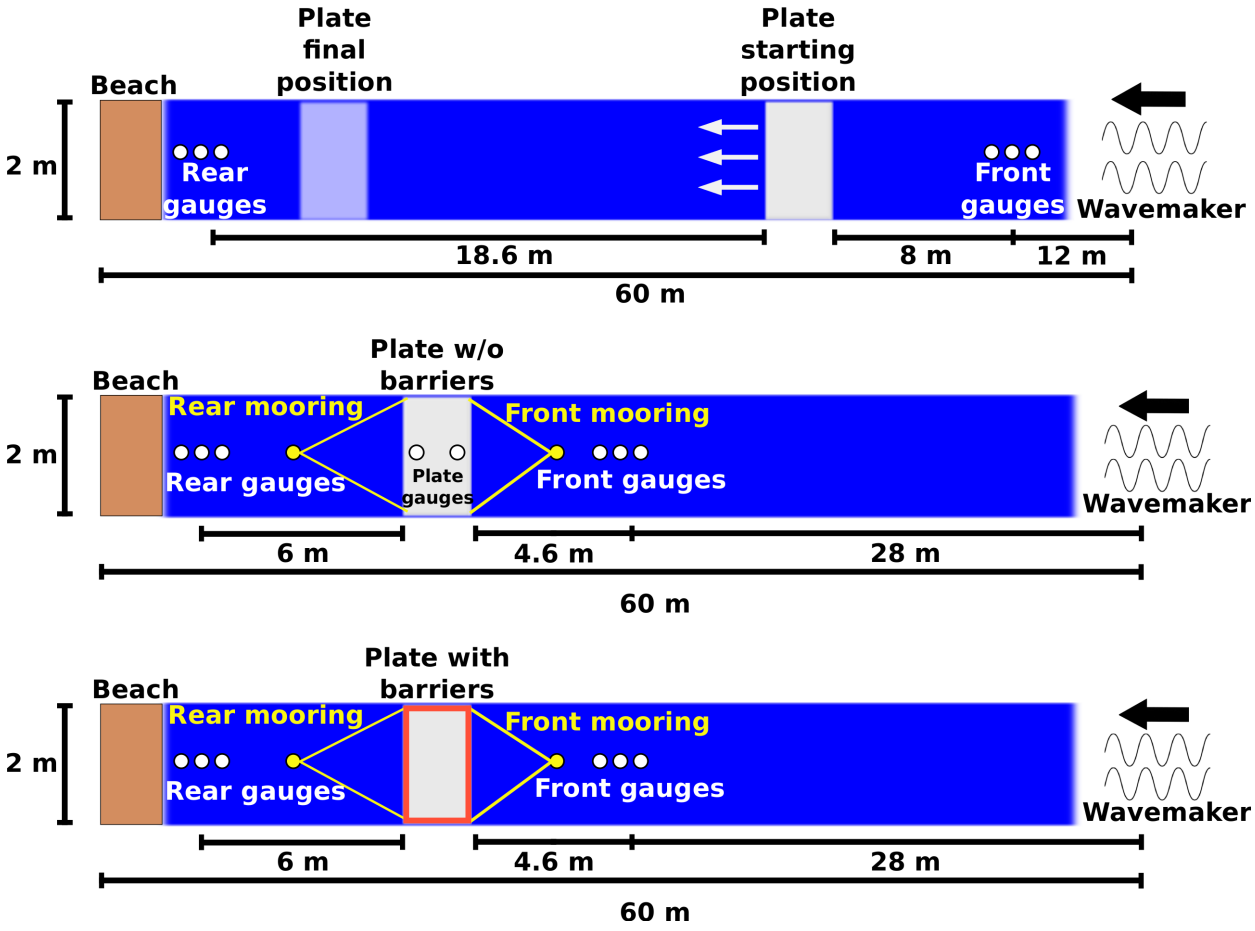

Figure 2: Schematic plan views of the three test cases (not to scale): freely floating (top panel); moored without barriers (middle); and moored with barriers (bottom).

0.06, 0.08, 0.1, 0.12 and 0.15, ranging from gently-sloping ($ka = 0.06$ and 0.08) to storm-like waves ($ka = 0.1$ to 0.15). In order to get benchmark measurements of the incident waves, tests without the plate were performed. Note that none of these waves are steep enough to reach the breaking onset (Babanin et al., 2007, Toffoli et al., 2010). Each test was performed three times to assess repeatability and uncertainties.

Records of the water surface elevation, η, were gathered with capacitance wave gauges, operating at a sampling frequency of 1000 Hz. Fig. 2 shows the locations of the gauges for the three different configurations. An array of three collinear probes was installed between the wave-make and the plate to measure the front field (incident and reflected waves), while a second three-probes array was deployed between the plate and the beach to measure the rear field (transmitted waves). The probes were located along the centreline of the tank to avoid wall effects. For the freely floating configuration, the front-field array was deployed 12 m from the wave-maker, and the rear-field array 39.6 m from the wave-maker — the distance between the two arrays ensured enough space for the plate to drift without colliding with the gauges. For the configurations involving moored plates, the front-field

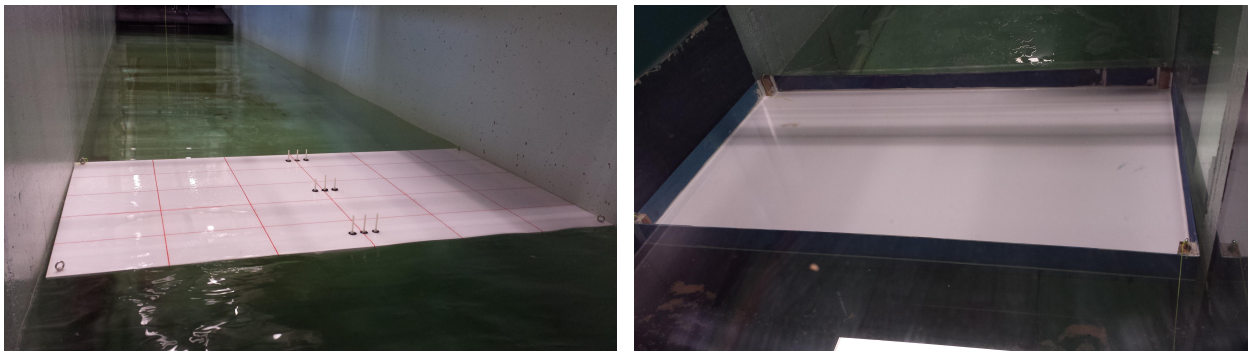

Figure 3: PVC plate in the moored case (left-hand panel) and moored with barriers case (right).

array was installed 28 m from the wave-maker and the rear-field array 40 m from the wave-maker. In the moored-without-barriers cases, a line of gauges (two for the PP plate, three for the PVC plate) was mounted on the plates to measure the overwash depth, although this data isn't analysed in this study.

The surface elevation was recorded for a maximum of 90 s. The first 50 s of the time series were used for processing to exclude contamination with reflected waves from the beach. To eliminate noise, a smoothed signal was generated by filtering components with frequencies smaller than 0.5 and greater than 3.5 times the frequency of the incident wave. Wave periods and amplitudes were calculated from the smoothed signal using a zero-crossing analysis (a standard procedure for signal analysis, e.g. Emery and Thomson, 2001). This involves determining the times at which the surface displacement crosses the zero, and finding the modulus of the extremal value between subsequent crossings, which is identified as an amplitude, with the time between successive amplitudes maxima or minima as periods.

A Discrete Fourier Transform was applied to the recorded surface elevation to approximate the wave energy spectrum

$$S(f) = \frac{1}{2}\int_0^\infty \hat{a}^2 \mathrm{d}f \tag{3}$$

where $f = 1/\tau = \omega/2\pi$ is wave frequency and $\hat{a}(f)$ is the amplitude of the component of the wave field at frequency f (Holthuijsen, 2010). The spectrum was evaluated as an ensemble average over non-overlapping windows of 8192 points. The reflection and transmission coefficients, R and T, respectively, were calculated as

$$R = \frac{|m_{0,\mathrm{front}} - m_{0,\mathrm{inc}}|}{m_{0,\mathrm{inc}}} \quad \text{and} \quad T = \frac{|m_{0,\mathrm{rear}}|}{m_{0,\mathrm{inc}}}, \tag{4}$$

where

$$m_0 = \int_0^\infty S(f)\,\mathrm{d}f, \tag{5}$$

is the zeroth-order moment of the wave spectrum $S(f)$ in the for the front, rear and incident fields.

3. Water surface elevations for wave period $\tau = 0.9\,\mathrm{s}$

3.1. The front field

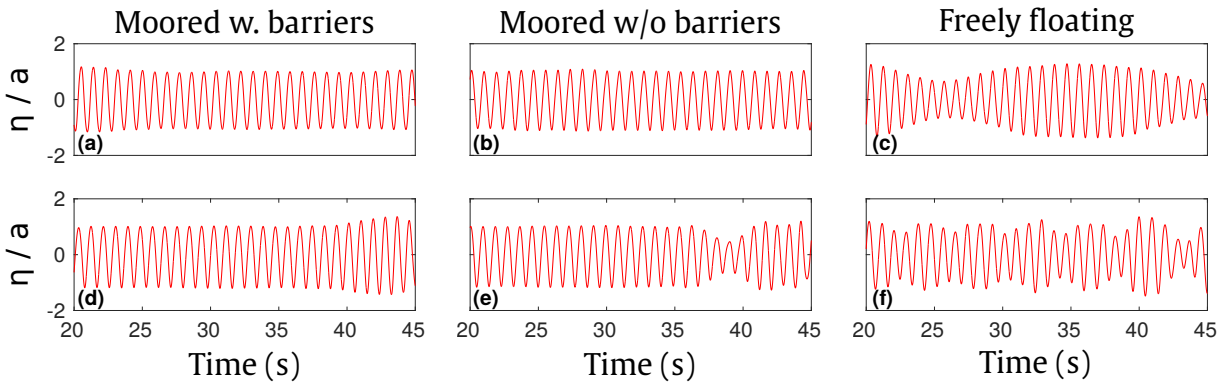

Figure 4: Examples of front-field free-surface elevation, recorded from the first probe, normalised with respect to incident wave amplitude for PP plate and incident wave period $\tau = 0.9\,\mathrm{s}$. Top panels (a,b,c) show typical wave elevations for mild incident waves, with $ka = 0.06$, and bottom panels for storm-like incident waves, with $ka = 0.15$. Left-hand panels (a,d) show the moored case with barriers, middle panels (b,e) the moored case without barriers, and right-hand panels (c,f) the freely floating case.

Fig. 4 shows 25 s time windows of surface elevations in the front field produced by the PP plate for the three configurations, and for the mildest steepness, $ka = 0.06$, and most storm-like steepness, $ka = 0.15$. For the mild steepness, the front fields produced by both moored plates retain the regular profile of the incident field. The freely floating plate slowly drifts down the flume, so that the reflection source is moving away from the front gauges, producing a surface elevation in the form of a sinusoid at a period approximately that of the incident period but modulated by a slowly varying envelope.

For the storm-like incident wave field, the elevation produced by the moored plate with barriers is regular for the first 20 s of the chosen window, but slightly increases in amplitude in the final 5 s, indicating some irregularity. This weak irregularity is potentially caused by occasional slamming of the plate ends against the water surface.

The elevation produced by the moored plate without barriers is regular for the first 15 s of the window, but shows significant irregularity in the final 10 s, which is attributed, at least in part, to strong overwash. Overwash is generated by the wave elevation rising above the ends of the plate, as described in Bennetts and Williams (2015). The strongest overwash occurs when the end of the plate closest to the wave-maker pitches downwards as the wave crest reaches it (i.e. the point at which the surface elevation is highest above the plate end), changing the reflection characteristics of the plate.

For the freely floating plate and the larger incident steepness, the elevation is highly irregular. This is partially attributed to modulation caused by drift — noting that the plate drifts faster for the larger incident steepness. Irregularity is also attributed to overwash, although the overwash is weaker for the drifting plate than the moored plate without barriers.

Fig. 5 shows photos of overwash of the moored PP plate without barriers taken by a camera mounted on the plate and facing the wave-maker. The left-hand panel is for the

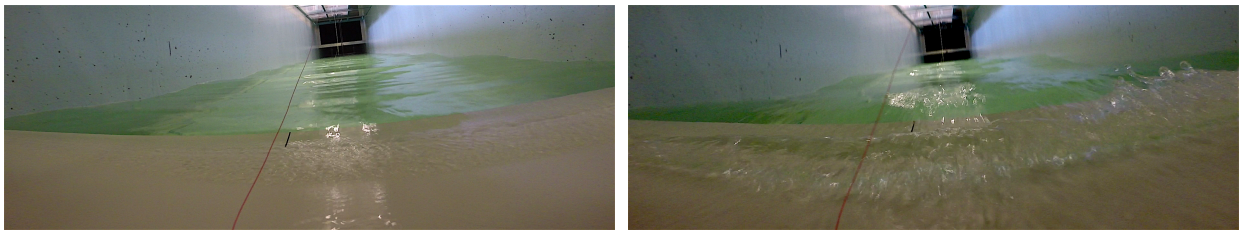

Figure 5: Photos showing overwash of PP plate by incident waves of period $\tau = 0.9\,\mathrm{s}$ taken by camera mounted on the centre of the plate facing the wave-maker, for incident steepness $ka = 0.06$ (left-hand panel) and $ka = 0.15$ (right).

mildest incident wave, $ka = 0.06$, for which the overwash is weak (relatively shallow and non-energetic). The right-hand panel is for the most storm-like incident wave, $ka = 0.15$, for which the overwash is strong (deep and energetic). Note, in particular, wave breaking in the overwash in this case.

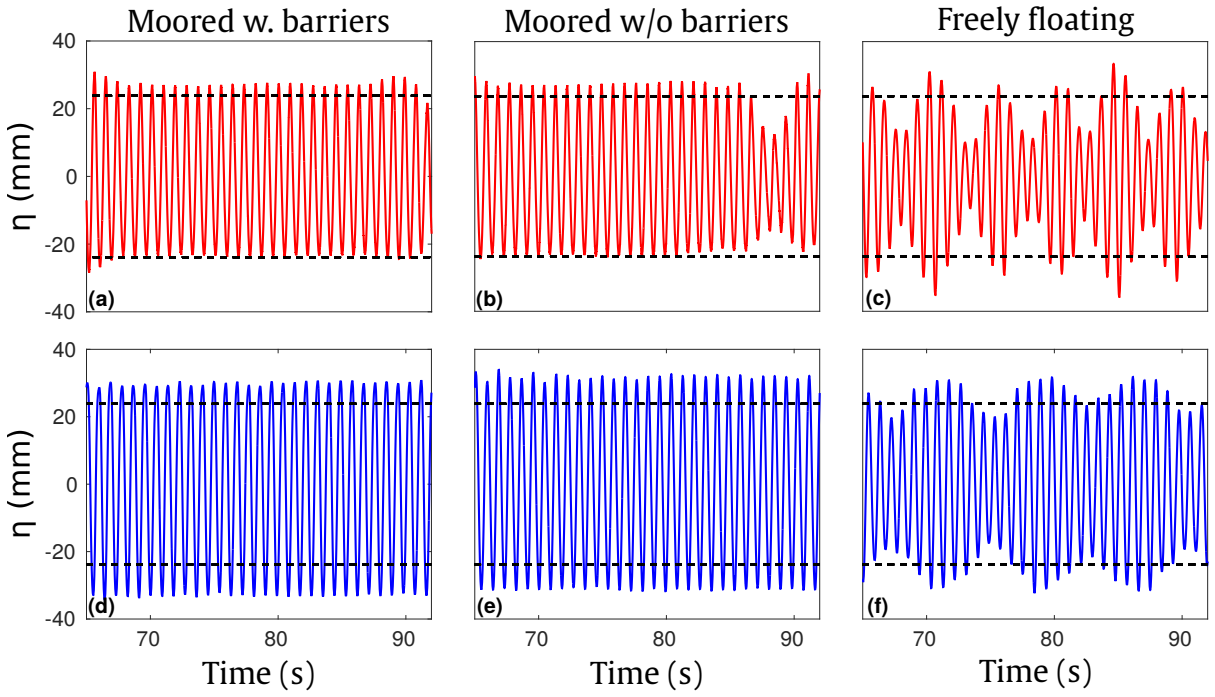

Figure 6: Examples of front-field free-surface elevation for incident wave with period $\tau = 0.9\,\mathrm{s}$ and steepness $ka = 0.12$. Results for PP plates are shown in top panels (a–c, —), and for PVC plate in bottom panels (d–f, —). Left-hand panels (a,d) show the moored case with barriers, middle panels (b,e) the moored case without barriers, and right-hand panels (c,f) the freely floating case. Black dashed lines represent the peak-to-trough amplitude of the incident waves.

Fig. 6 shows typical examples of water surface elevations in the front field, for the two different plastics and three different configurations, and a storm-like incident steepness $ka = 0.12$. The peak-to-trough amplitude of the incident field is superimposed on the plots, and

it is evident that the front-field amplitude is consistently larger than that of the incident field. The amplitude is largest for the PVC plate, suggesting it reflects a greater proportion of the incident wave than the than PP plate.

The irregularity of the front field produced by the moored PP plate without barriers is again evident. However, the front field produced by the moored PVC plate without barriers is regular. This difference is attributed to the PP plate experiencing stronger overwash than the PVC plate, because it has a higher density giving it a smaller freeboard. For the tests shown, the mean overwash depth of the PP plate (measured by the gauges mounted on the plate) was $\sim 17\,\mathrm{mm}$, whereas it was only $\sim 4\,\mathrm{mm}$ for the PVC plate.

Similarly to the profile shown in Fig. 4(f) for the largest incident wave steepness, the front field elevation for the freely floating PP plate displays strong irregularity that cannot be attributed to modulation alone (albeit slightly weaker than the irregularity for the steeper incident wave). For the freely floating PVC plate, the irregularity is far weaker, being dominated by smooth modulation. This is again attributed to weaker overwash of the PVC plate, noting that the PP plate also drifts faster than the PVC plate.

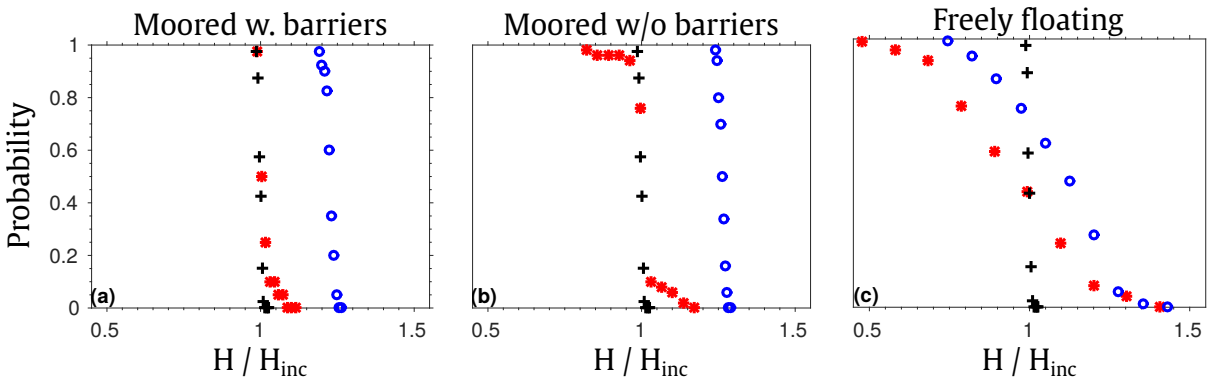

Figure 7: Probability of front-field wave heights exceeding H/H_{inc}, for tests shown in Fig. 6 ($\tau = 0.9\,s$ and $ka = 0.12$). Results for PP plate ($*$) and PVC plate ($\circ$), with configuration of a (a) moored plate with barriers, (b) moored plate without barriers, and (c) freely floating plate. Results for the incident wave field ($+$) are included for reference.

Fig. 7 shows the regularity/irregularity of the wave height, $H = 2a$, in terms of the probability $P(H > H_0)$ of exceeding a given height H_0 (e.g. Ochi, 1998) for the tests shown in Fig. 6 (over the full 50 s series rather than the sample windows) and the incident wave field from the benchmark tests. The probability for the incident wave is approximately a vertical line, indicating little variability, as expected due to it being regular. The probabilities for the front fields indicate that the wave heights produced by the PVC plates in the front field are regular (little variation in wave heights) and greater than those produced by the PP plates in the corresponding cases. They also show irregularity of the front fields produced by the freely floating plates (wide spread of wave heights), although noting that the probabilities are smooth.

For the moored PP plate without barriers, most wave heights cluster around a value slightly greater than unity. However, significant proportions of wave heights deviate from

this value, both above it and below it, indicating irregularity. For the moored PP plate with barriers, the only deviation from regularity is a proportion of $\sim 10\,\%$ of the wave heights that exceed the regular height, similar to the increase in wave amplitudes observed in the final 5 s of the time series in Fig. 6(d), attributed to occasional slamming of the plate ends against the water surface. The strength of the slamming was weaker for the moored PVC plate with barriers (consistent with the observations of Bennetts et al., 2015), and the corresponding time series and wave-height distribution do not display the increase in wave amplitudes/heights.

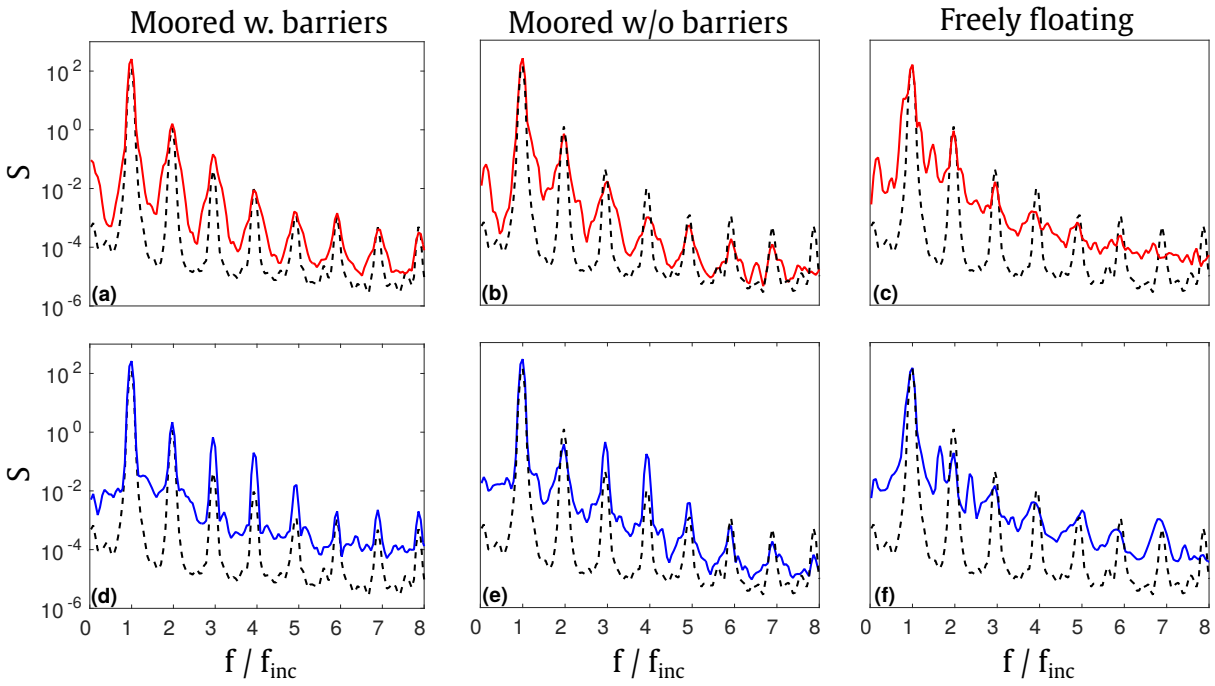

Figure 8: Wave spectra in the front field, corresponding to Fig. 6 ($\tau = 0.9\,\mathrm{s}$ and $ka = 0.12$) for the PP plate (a–c,—) and PVC plate (d–f,—), as functions of frequency, f, normalised with respect to the incident frequency, f_{inc}. The spectrum of the incident wave field is superimposed (--).

Fig. 8 shows the wave spectrum, S given in Eqn. (3), for each of the tests shown in Fig. 6 (again over the 50 s record). The spectra are shown as functions of frequency, normalised by the incident frequency $f_{\mathrm{inc}} = 1/0.9\,\mathrm{s}^{-1}$. The incident wave spectrum is superimposed for comparison. Its largest peak is at the incident frequency $f/f_{\mathrm{inc}} = 1$, with subsequent peaks at the higher harmonics $f/f_{\mathrm{inc}} = n \in \mathbb{N}$ $(n > 1)$, which decrease in amplitude as n increases. The harmonics define the bound modes, inevitable even in regular waves due to nonlinearities.

The spectra for the freely floating plates show the significant irregularity noted in Fig. 6(c,f) and Fig. 7(c). The harmonic structure of the incident field is smeared by the reflected field, with the highest harmonics imperceptible for the PP plate. The majority of wave energy is still centred around the fundamental frequency ($f/f_{\mathrm{inc}} = 1$), but is spread, with sidebands appearing, particularly for the PP plate.

The moored PVC plates approximately retain the harmonic structure of the incident spectrum, with the fundamental harmonic still narrow-banded, and the second harmonic likewise for the plate with barriers. The third to fifth harmonics gain energy, implying these higher harmonics are strongly reflected by the plate or that reflection by the plate involves a transfer of wave energy between harmonics. The moored PP plates display irregularity in the form of energy spreading around the harmonics (although not to the extent of the freely floating plates). The greater irregularity seen in the profiles for the plate without barriers — attributed to strong overwash — manifests as larger spread of energy between the fundamental and second harmonics.

3.2. The rear field

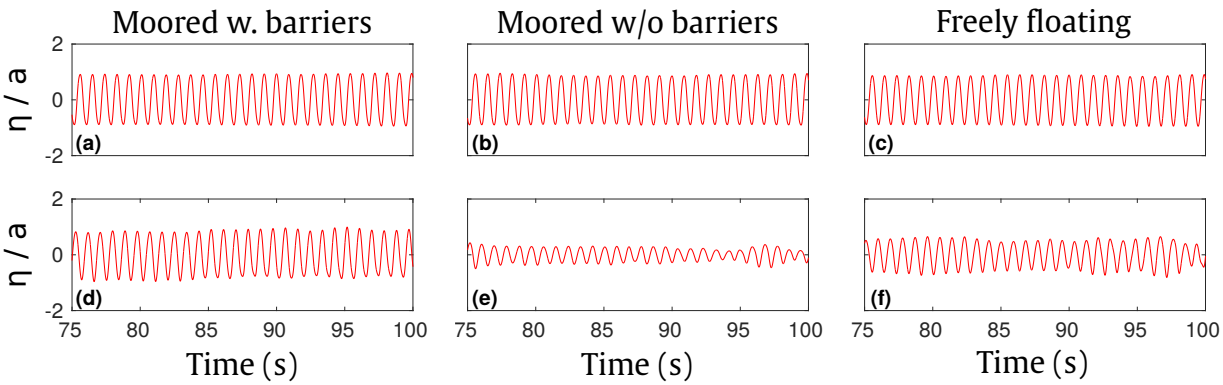

Figure 9: As in Fig. 4 but for the rear field.

Fig. 9 shows the free-surface elevations for transmitted waves in the rear field corresponding to the front field elevations shown in Fig. 4, i.e. $\tau = 0.9\,\mathrm{s}$, and $ka = 0.06$ and 0.15. In this case, for the mild incident wave, $ka = 0.06$, the rear fields for all three configurations are very similar and regular, as the transmitted field is dominated by the incident field. For the storm-like incident wave, $ka = 0.15$, the rear field for the plate with barriers is similar to that for the mild incident wave, although with a small degree of irregularity evident in the amplitudes. The effect of increasing the incident steepness is striking for the plates without barriers. Both have attenuated amplitudes and become highly irregular. This is again attributed to strong overwash in these cases, with, for example, the water running off the plate surface injecting high-frequency wave components into the transmitted wave field. Attenuation and irregularity are most pronounced for the moored plate because it experiences stronger overwash than the freely floating plate, as noted in §3.1.

Fig. 10 shows the free-surface elevations in the rear field for the two plastics and all three configurations, with an incident steepness of $ka = 0.12$. For both plastics and all three test configurations, the amplitudes in the rear field are less than the incident wave amplitude, as expected. The amplitudes are larger for the PVC plates than the PP plates, indicating that the PVC plates transmit a greater proportion of the incident wave field than the PP plates, although the opposite may have been expected, as the results shown in § 3.1 appeared to show that the PVC plates reflect a greater proportion of the incident wave field than the PP

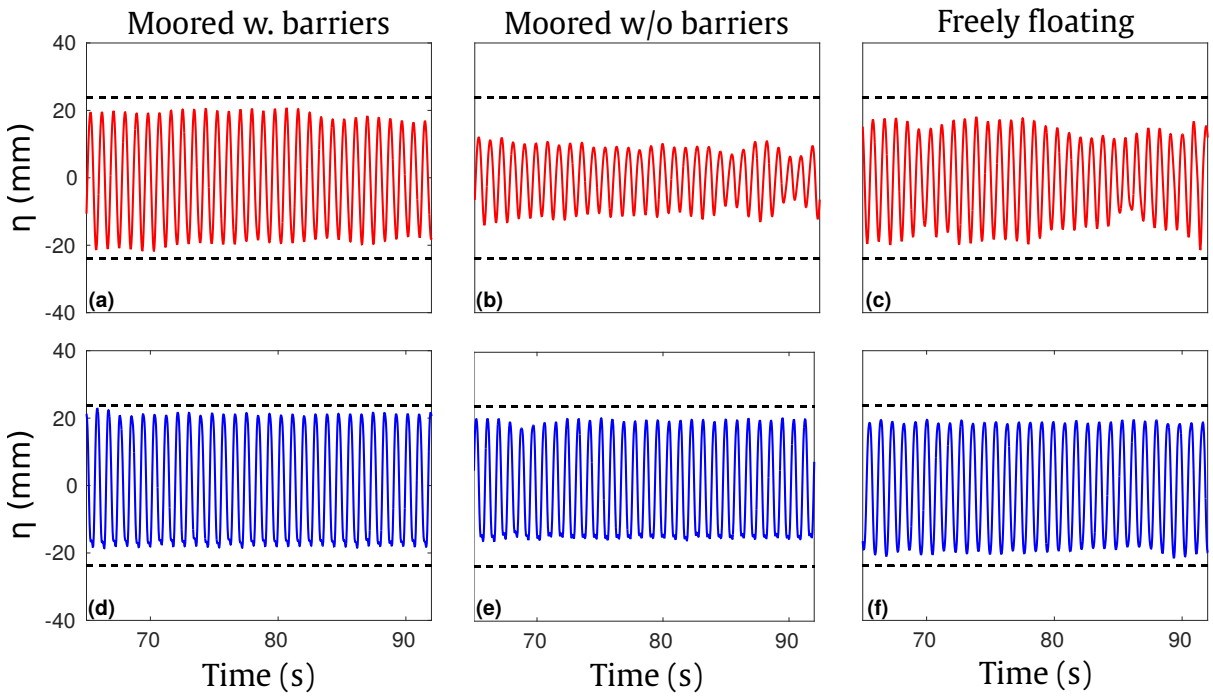

Figure 10: As in Fig. 6 but for the rear field.

plates. The PVC plates without barriers display far less attenuation and irregularity than the PP plates. Again, this is attributed to the larger freeboard of the PVC plates meaning they experience weaker overwash than the PP plates.

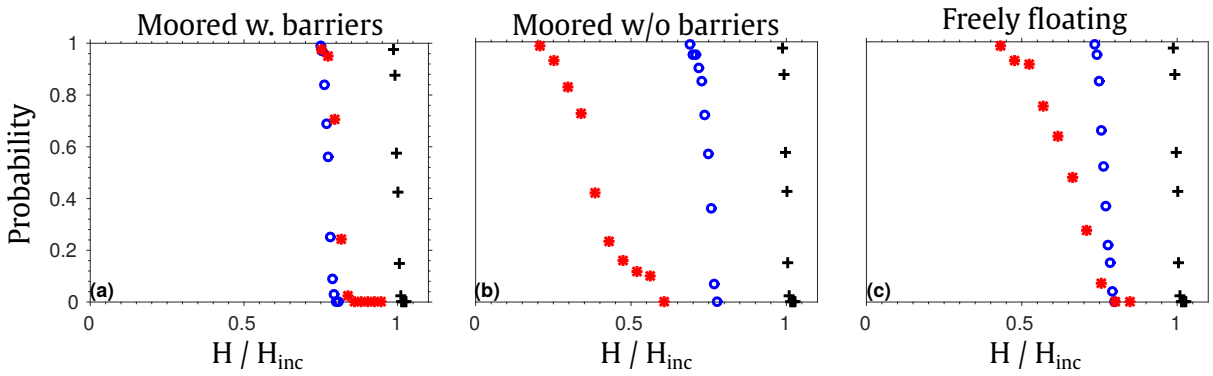

Figure 11: As in Fig. 7 but for the rear field.

Fig. 11 shows the wave height exceedance probabilities for the rear fields considered in Fig. 10. It confirms that the rear fields produced by the PVC plates are (at least approximately) regular, with the strongest deviation being for the moored plates without barriers. The moored PP plate with barriers is essentially regular, but, as in the front field, displays some heights that exceed the regular value. The PP plates without barriers both produce wide ranges of wave heights, particularly the moored plate.

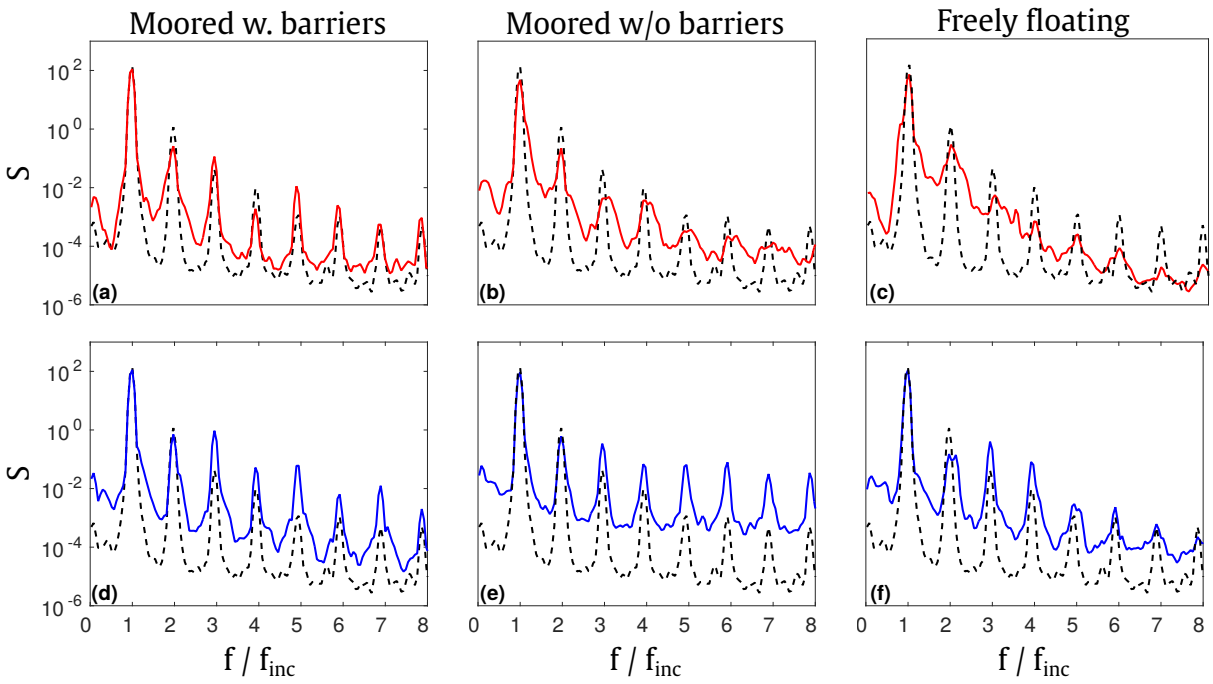

Figure 12: As in Fig. 8 but for the rear field.

Fig. 12 shows the corresponding wave spectra, with the incident spectrum superimposed. The most significant smearing of the harmonic structure is for the PP plates without barriers, particularly the freely floating plate. In all cases the fundamental harmonic loses energy with respect to the the incident spectra. Again, this is most significant for the PP plates without barriers, where sidebands appear around the fundamental harmonic.

4. Reflection and transmission coefficients and dissipation

Fig. 13 shows the reflection coefficient, R, as a function of the incident wave steepness, for both plastics and all three configurations. Error bars, equivalent to two times the standard deviation (i.e. 95 % confidence intervals), show the sample variability. The data are slightly offset with respect to the incident steepness for the sake of clarity. Predictions given by a coupled potential-flow and thin-plate theoretical model are superimposed for reference (see § 1, and Toffoli et al., 2015), noting that the model is based on linear theory, so that it is constant with respect to wave steepness.

On average, reflection coefficients decrease with increasing wave period (reading each rows of panels left to right) and are insensitive to wave steepness, consistent with model predictions. The freely floating plates generally produces the weakest reflection, which is attributed to drift of the plate providing less resistance to the incident waves. The moored plates with barriers generally produce the strongest reflection (although only marginally greater than the moored plates without barriers), which is attributed to the barriers resisting incident waves washing over the plates.

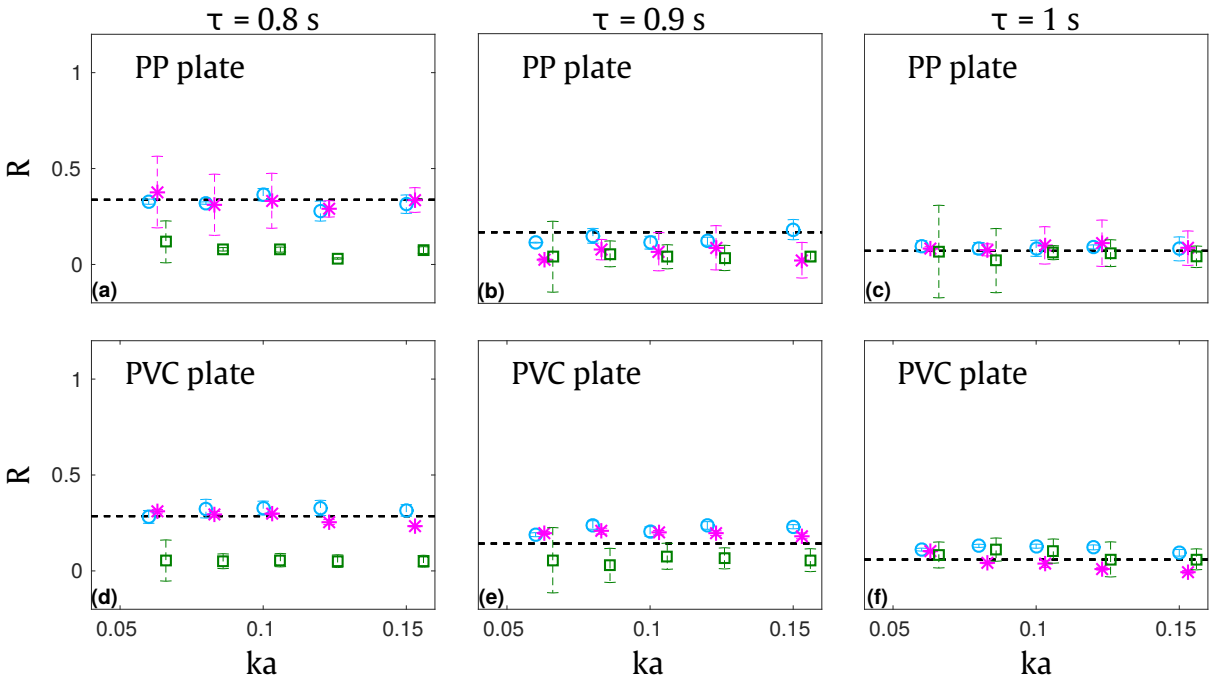

Figure 13: Reflection coefficient, as a function of the incident wave steepness, for the mooring-with-barriers case (○), mooring-without-barriers case (∗), and freely floating case (□). Whiskers indicate the 95 % confidence intervals. Linear theoretical model predictions are superimposed (--).

For the longest period, $\tau = 1\,\mathrm{s}$, which results in the weakest reflection on average for all plates, and the PP plate, the reflection coefficients produced by the different configurations are almost identical, and the model accurately predicts their values. The freely floating plate displays significant variability for the least steep incident waves, which can be partially attributed to larger measurement errors relative to amplitudes. For the PVC plate, the reflection coefficients produced by the different configurations are similar, although they are smallest for the moored-without-barriers case for all but the smallest steepness, and largest for the moored-with-barriers case for all steepnesses. On average, the model slightly under predicts the reflection.

For the intermediate wave period, $\tau = 0.9\,\mathrm{s}$, and the PP plates, although the reflection coefficients produced by the different configurations are similar, there is a general trend for the moored-with-barriers case to produce the strongest reflection, and the freely floating case to produce the weakest reflection. These trends are stronger for the PVC plates, particularly for the freely floating plate to produce the weakest reflection — the reflection produced by the moored plates are still similar. The model over predicts the reflection coefficients for the PP plates and the freely floating PVC plate, but slightly under predicts the reflection produced by the moored PVC plates.

For the shortest period, $\tau = 0.8\,\mathrm{s}$, which results in the strongest reflection overall, the reflection coefficients for the moored plates are almost identical, and their values are accurately predicted by the model. The reflection produced by the freely floating plates is significantly weaker than the moored plates. Moreover, the reflection coefficients for the

freely floating plates barely increase as the incident period decreases.

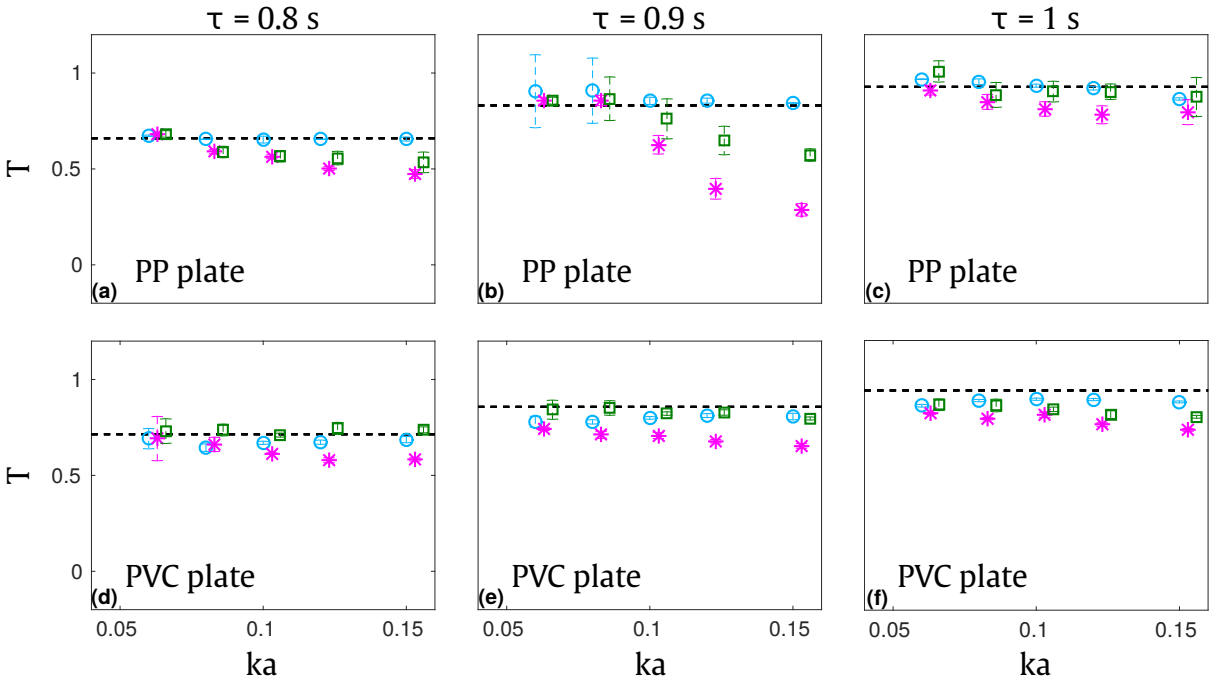

Figure 14: As in Fig. 13, but for the transmission coefficient.

Fig. 14 shows the corresponding results for the transmission coefficient, T. On average (with respect to incident steepness), transmission increases as the incident period increases, consistent with model predictions. For the moored-with-barriers cases, the transmission coefficients are largely insensitive to the incident steepness, and the model predictions are generally accurate, although they slightly over predict transmission for the PVC plate.

For the cases without barriers, the transmission coefficients tend to decrease with increasing incident steepness — Toffoli et al. (2015) reported a similar phenomenon for the unmoored PP plate. The decrease is stronger for the moored plates than the freely floating plates, and the PP plates than the PVC plates, and is strongest at the 0.9 s period. It is attributed to wave breaking in the overwash region dissipating wave energy — as the incident wave becomes steeper, the overwash becomes stronger and the dissipation increases. The transmission coefficient for the PP plates are affected by the dissipation more than the PVC plates, because, as noted above, the PP plates experience stronger overwash than the PVC plates. Similarly, the transmission coefficient for the moored plates are affected more than the freely floating plates because they experience stronger overwash.

Fig. 15 provides evidence that the decrease in the transmission coefficient as the incident wave becomes steeper is caused by energy dissipation, It shows the sums of corresponding reflection and transmission coefficients, $R + T$. Conservation of wave energy would be indicated by $R + T = 1$, as given by the model. The moored-with-barriers cases satisfy this conservation identity approximately for all incident wave periods and steepnesses. The values of $R+T$ for the cases without barriers tend to decrease as the incident wave steepness

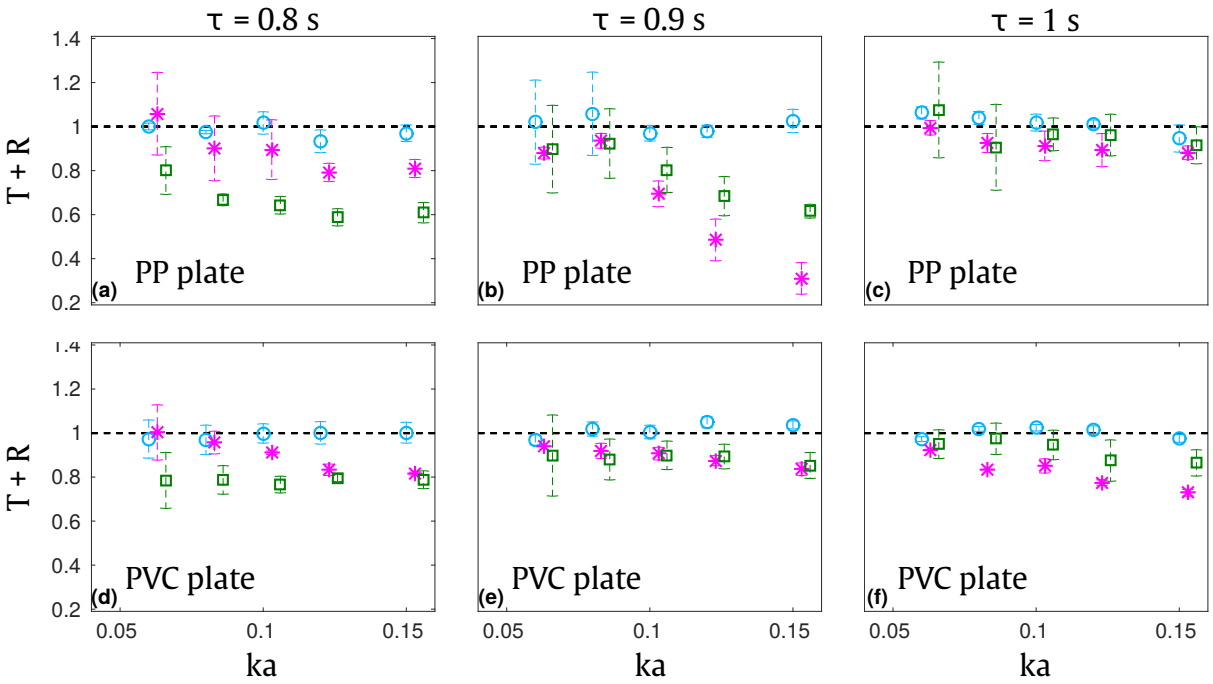

Figure 15: Sums of corresponding reflection and transmission coefficients shown in Figs. 13–14.

increases, consistent with the findings for the transmission coefficient. The dissipation is as significant as $\sim 70\,\%$ for the moored PP plate without barriers when $\tau = 0.9\,\mathrm{s}$ and $ka = 0.15$. For the shortest incident period, $\tau = 0.8\,\mathrm{s}$, the dissipation is most significant for the freely floating plates, and this coincides with the period at which the plates experience the fastest drift.

5. Conclusions

Analysis of reflection and transmission of regular incident water waves by a thin floating plate during laboratory wave-flume experiments has been reported. A plastic sheet acted as the thin plate, and two plastics were tested (a more rigid and dense PP and a more flexible and less dense PVC). Three different deployment configurations were adopted: one in which the plate was moored and barriers were attached to its edge to suppress overwash; one in which the plate was moored without barriers, permitting overwash; and one in which the plate was unmoored and free to drift — thus testing the impacts of drift and overwash on reflection and transmission. A range of incident wave periods and steepnesses were tested, and reflection and transmission coefficients were compared to predictions for a linear theoretical model based on coupled potential-flow and thin-plate theories.

The main results are summarised as follows:

1. For the moored plates with barriers, both the front (incident plus reflected) field and the rear (transmitted) field were shown generally to retain the regular cross-sectional profile of the incident wave field, although some evidence of irregularity was noted in

the form of intervals of slightly increased amplitudes for the denser PP plate. The theoretical model was shown to predict the reflection and transmission coefficients with reasonable accuracy, and no evidence of significant energy dissipation was found.

2. For the moored plates without barriers, the front and rear fields were shown to become irregular as the incident wave steepness increases, particularly the rear field, for which the amplitude relative to the incident amplitude was shown to attenuate as incident steepness increases, particularly for the PP plate. This was attributed to strong overwash of the plates for steep incident waves. The attenuation was shown to be caused by wave energy dissipation, not included in the theoretical model, which was hypothesised to be due to wave breaking in the overwash region.
3. For the freely floating plates, the front fields were shown to be of the form of sinusoids modulated by slowly varying envelopes, which was attributed to the plates drifting. Similarly to the case of moored plates without barriers, the rear fields were found to be regular for mild incident waves, but irregular for storm-like incident waves and with attenuated amplitudes. These effects were observed to be weaker than the moored-with-barriers case, and this was related to weaker overwash of the freely floating plates than the corresponding moored plates.

The findings suggest that reflection and transmission of regular waves by thin floating plates are affected by overwash and drift of the plates for incident steepnesses greater than $ka \sim 0.08$. For regions of the ice-covered ocean composed of floes with horizontal dimensions comparable to wavelengths — where waves are free to wash over floes, and the floes to drift, depending on resistance provided by surrounding floes — these findings imply that the linear theoretical model may be suitable to model wave attenuation for relatively mild incident waves only. Further, the results indicate that overwash, in particular, is responsible for wave energy dissipation and transfer of wave energy to higher frequencies, motivating development of theoretical/numerical models that incorporate these phenomena.

6. Acknowledgements

The Universities of Melbourne and Newcastle funded the experiments. FN is supported by a Swinburne University of Technology Postgraduate Research Award. The Australian Research Council funds an early-career fellowship for LGB (DE130101571) and a mid-career fellowship for JPM (FT120100409). The Australian Antarctic Science Program provides support for LGB and a PhD top-up scholarship for DMS (project 4123). MHM acknowledges support from the U.S. Office of Naval Research (project N00014-13-1-0290).

References

Babanin, A., Chalikov, D., Young, I., Savelyev, I., 2007. Predicting the breaking onset of surface water waves. Geophys. Res. Lett. 34 (7).

Bennetts, L. G., Alberello, A., Meylan, M. H., Cavaliere, C., Babanin, A. V., Toffoli, A., 2015. An idealised experimental model of ocean surface wave transmission by an ice floe. Ocean Model. 96(1), 85–92.

Bennetts, L. G., Biggs, N. R. T., Porter, D., 2007. A multi-mode approximation to wave scattering by ice sheets of varying thickness. J. Fluid Mech. 579, 413–443.

Bennetts, L. G., Squire, V. A., 2012. On the calculation of an attenuation coefficient for transects of ice-covered ocean. Proc. R. Soc. A 468, 136–162.

Bennetts, L. G., Williams, T. D., 2010. Wave scattering by ice floes and polynyas of arbitrary shape. J. Fluid Mech. 662, 5–35.

Bennetts, L. G., Williams, T. D., 2015. Water wave transmission by an array of floating disks. Proc. R. Soc. A 471 (2173).

Deshpande, V., Fleck, N., 2001. Multi-axial yield behaviour of polymer foams. Acta Mater. 49 (10), 1859 – 1866.

Emery, W., Thomson, R., 2001. Data analysis methods in physical oceanography. Advanced series on ocean engineering - vol. 2. Elsevier Science B.V., Amsterdam.

Holthuijsen, L. H., 2010. Waves in oceanic and coastal waters. Cambridge University Press.

Massom, R., Stammerjohn, S., 2010. Antarctic sea ice variability: physical and ecological implications. Polar Sci. 4, 149–458.

Masson, D. A., LeBlond, P., 1989. Spectral evolution of wind-generated surface gravity waves in a dispersed ice field. J. Fluid Mech. 202, 43–81.

McGovern, D. J., Bai, W., 2014. Experimental study on kinematics of sea ice floes in regular waves. Cold Reg. Sci. Technol. 103, 15–30.

Meylan, M. H., Bennetts, L. G., Cavaliere, C., Alberello, A., Toffoli, A., 2015. Experimental and theoretical models of wave-induced flexure of a sea ice floe. Phys. Fluids 27 (4).

Meylan, M. H., Bennetts, L. G., Kohout, A. L., 2014. In situ measurements and analysis of ocean waves in the Antarctic marginal ice zone. Geophys. Res. Lett. 41, 1–6.

Meylan, M. H., Squire, V. A., 1994. The response of ice floes to ocean waves. J. Geophys. Res. 99 (C1), 891–900.

Meylan, M. H., Squire, V. A., 1996. Response of a circular ice floe to ocean waves. J. Geophys. Res. 101, 8869–8884.

Montiel, F., Bennetts, L. G., Squire, V. A., 2012. The transient response of floating elastic plates to wave-maker forcing in two dimensions. J. Fluids Struct. 28, 416–433.

Montiel, F., Bennetts, L. G., Squire, V. A., Bonnefoy, F., Ferrant, P., 2013a. Hydroelastic response of floating elastic discs to regular waves. Part 2. Modal analysis. J. Fluid Mech. 723, 629–652.

Montiel, F., Bonnefoy, F., Ferrant, P., Bennetts, L. G., Squire, V. A., Marsault, P., 2013b. Hydroelastic response of floating elastic discs to regular waves. Part 1. Wave basin experiments. J. Fluid Mech. 723, 604–628.

Newman, S., Strella, S., 1965. Stress-strain behavior of rubber-reinforced glassy polymers. J. Appl. Polym Sci. 9 (6), 2297–2310.

Ochi, M. K., 1998. Ocean waves: the stochastic approach. Cambridge University Press, Cambridge.

Shokrieh, M. M., Joneidi, V. A., Mosalmani, R., 2015. Characterization and simulation of tensile behavior of graphene/polypropylene nanocomposites using a novel strain-rate-dependent micromechanics model. J. Thermoplast. Compos. 28 (6), 818–834.

Skene, D. M., Bennetts, L. G., Meylan, M. H., Toffoli, A., 2015. Modelling water wave overwash of a thin floating plate. J. Fluid Mech. 777, R3.

Smith, M. J. A., Meylan, M. H., 2011. Wave scattering by an ice floe of variable thickness. Cold Reg. Sci. Technol. 67 (1-2), 24–30.

Sree, D., Law, A. W.-K., Shen, H. H., 2016. An experimental study on the interactions between surface waves and floating viscoelastic covers. Wave Motion, accepted.

Toffoli, A., Babanin, A. V., Onorato, M., Waseda, T., 2010. Maximum steepness of oceanic waves: Field and laboratory experiments. Geophys. Res. Lett. 37 (5).

Toffoli, A., Bennetts, L. G., Meylan, M. H., Cavaliere, C., Alberello, A., Elsnab, J., Monty, J. P., 2015. Sea ice floes dissipate the energy of steep ocean waves. Geophys. Res. Lett. 42 (20), 8547–8554.

Williams, T. D., Bennetts, L. G., Squire, V. A., Dumont, D., Bertino, L., 2013a. Wave-ice interactions in the marginal ice zone. Part 1: Theoretical foundations. Ocean Model. 71, 81–91.

Williams, T. D., Bennetts, L. G., Squire, V. A., Dumont, D., Bertino, L., 2013b. Wave-ice interactions in

the marginal ice zone. Part 2: Numerical implementation and sensitivity studies along 1D transects of the ocean surface. Ocean Model. 71, 92–101.

Yiew, L. J., Bennetts, L. G., Meylan, M. H., French, B. J., Thomas, G. A., 2016. Hydrodynamic responses of a thin floating disk to regular waves. Ocean Model. 97, 52–64.